Internal Medicine
The Japanese Society of Internal Medicine
doi: 10.2169/internalmedicine.6653-20
Intern Med 60: 2395-2403, 2021
http://internmed.jp

【 ORIGINAL ARTICLE 】

"Computed Tomography Perihematomal Rims": A Perihematomal Low-Density Area Is a Part of an Acute Brain Hemorrhage

Takahiro Sato[1], Yasuhiro Nishiyama[1], Satoshi Suda[1], Takashi Shimoyama[1], Shiro Takahashi[1], Yuki Sakamoto[1], Junya Aoki[1], Kentaro Suzuki[1], Tetsuro Sekine[2], Shin-ichiro Kumita[2] and Kazumi Kimura[1]

Abstract:

Objective Computed tomography (CT) can be used for visualizing acute intracerebral hemorrhages (ICHs) as distinct hyperdense areas and cerebral edema as perihematomal low-density areas (LDAs). We observed a perihematomal LDA on CT, which appeared to be part of a hemorrhage on magnetic resonance imaging (MRI) in acute ICH. We named this "CT perihematomal rim" and evaluated its characteristics and clinical significance.

Methods We stratified patients with acute ICH according to the presence or absence of a CT perihematomal rim and then compared their radiologic findings. Logistic regression analyses were performed to assess whether the CT findings can predict the presence of a CT perihematomal rim.

Patients Patients within 24 hours of ICH onset who were admitted between September 1, 2014, and October 31, 2018, were registered.

Results Overall, 139 patients (91 men; mean age, 66 years) were investigated. CT perihematomal rims were observed in 40 patients (29%). ICH volumes on CT were 30% smaller than those on MRI in patients with CT perihematomal rims. On a multivariate analysis, the presence of a CT perihematomal rim was independently associated with the maximum diameter of the perihematomal LDA. According to a receiver operating characteristic analysis, the maximum LDA diameter threshold was 7.5 mm (sensitivity, 85%; specificity, 83%).

Conclusion CT perihematomal rims were observed in 29% of the patients with acute ICH. A perihematomal LDA (>7.5 mm) in acute ICH cases should be considered a CT perihematomal rim. Clinicians should be aware that the ICH volume on CT may be underestimated by 30%.

Key words: intracerebral hemorrhage, computed tomography, magnetic resonance imaging, perihematomal low-density area

(Intern Med 60: 2395-2403, 2021)
(DOI: 10.2169/internalmedicine.6653-20)

Introduction

Computed tomography (CT) is the gold standard for the diagnostic imaging of intracerebral hemorrhages (ICHs), as this imaging modality is simple and minimally invasive (1). ICH lesions appear on CT scans as well-defined, hyperdense areas (HDAs), and the hematoma volume is calculated using a formula based on the size of the HDA (the ABC/2 formula) (2). In contrast, ICH-associated edematous changes in the cerebral parenchyma appear as perihematomal low-density areas (LDAs) (3, 4).

[1]Department of Neurology, Graduate School of Medicine, Nippon Medical School, Japan and [2]Department of Radiology, Graduate School of Medicine, Nippon Medical School, Japan
Received for publication November 4, 2020; Accepted for publication December 26, 2020
Correspondence to Dr. Yasuhiro Nishiyama, nomo16@nms.ac.jp

Conversely, magnetic resonance imaging (MRI) outperforms CT for the detection of primary hemorrhages owing to its strong paramagnetic effect on hemoglobin degradation products in the blood (5, 6). Gradient-recalled echo T2*-weighted imaging (T2*WI) is one of the most sensitive methods for visualizing blood components in all sequences (7-10). T2-weighted imaging (T2WI) is sensitive for the detection of acute ICH within 6 hours of onset (8, 10). Fluid-attenuated inversion recovery (FLAIR) imaging is another sensitive method for visualizing blood components, wherein an increase in signal intensity reflects a small amount of leaked blood (11). A study reported that the high detectability of acute ICH by MRI is comparable to that by CT (9); however, MRI is less accessible due to its high cost and the limited number of medical facilities equipped with MRI scanners internationally (12); therefore, studies examining MRI findings among patients with acute ICH remain limited.

We performed non-contrast CT of the head and MRI of the brain within 2 hours apart for patients with acute ICH. We observed the presence of "perihematomal LDAs on CT that appeared to be part of hemorrhages on MRI." Hemorrhages on MRI were almost indistinguishable from perihematomal LDAs which corresponds to cerebral edema on CT; however, perihematomal LDAs were located inside the hypo-intense rim at the edge of the hematoma on MRI. Additionally, CT and MRI resulted in different visual representations of the ICH lesions. We hypothesized that the perihematomal LDAs on CT, which were previously thought to be cerebral edema, might also be a part of hematomas and named the above perihematomal LDA finding the "CT perihematomal rim." This study aimed to investigate the imaging characteristics of the CT perihematomal rim and the association with other imaging findings and clinical courses in patients with acute ICH.

Materials and Methods

Patient selection

The data supporting the findings of this study are available from the corresponding author on reasonable request. We conducted a retro-prospective, single-center, observational study, which was approved by the ethics committee of the Nippon Medical School and conformed to the tenets of the Declaration of Helsinki. All patients registered prospectively, or their family members provided written informed consent prior to study participation. For retrospectively registered patients, we posted a notice about this study on the homepage of our university hospital website, according to the rules of the ethics committee. We enrolled patients aged >18 years within 24 hours of acute spontaneous ICH onset (n=249) who were admitted to the Nippon Medical School Hospital between September 1, 2014, and October 31, 2018. Patients were included in the study if they had undergone non-contrast CT of the head and MRI of the brain in the same time window of admission. Patients were excluded if they had (a) any signs of secondary hemorrhage (such as hemorrhagic infarction, trauma, tumors, or vascular malformations); (b) a >2-hour time lag between CT and MRI scans; (c) not undergone all useful MRI sequences for visualizing the hemorrhagic lesion (i.e., T2WI, FLAIR imaging, and T2*WI); (d) not undergone either CT or MRI scans due to clinical reasons (such as severe symptoms); and (e) been examined using MRI scanners from different manufacturers. All patients were hospitalized in the stroke care unit and underwent active antihypertensive treatment by the continuous injection of the calcium antagonist (nicardipine). The target values for blood pressure management were below 140/90 mmHg for systolic blood pressure/diastolic blood pressure.

Baseline characteristics

The patients' background information, including age, sex, life history (smoking and alcohol use), disease history (hypertension, diabetes mellitus, dyslipidemia, and atrial fibrillation), and drug history (antiplatelet and anticoagulant drugs uses), was recorded (a detailed definition of each disease history is included in the Supplemental material). The serum C-reactive protein (CRP), plasma D-dimer, and plasma brain natriuretic peptide (BNP) levels were measured as indices of inflammatory changes, coagulability and cardiac function, respectively (13). The systolic and diastolic blood pressure (mmHg) were assessed as physiological measures on admission. The neurological status was assessed using the National Institutes of Health Stroke Scale (NIHSS) score. The functional outcome was assessed using the modified Rankin scale (mRS), and a poor clinical outcome was defined as an mRS grade of ≥4 at 3 months after ICH onset.

Neuroimaging

CT scans were performed using standard clinical parameters with a 5-mm axial section thickness, a 120-kV tube voltage, and a 100-mA tube current and they were recorded using an appropriate window width and level setting of 100/40 (LightSpeed VCT; GE Healthcare, Little Chalfont, UK). The MR images were acquired using a 1.5-Tesla scanner (Echelon OVAL; Hitachi, Tokyo, Japan), and scans were performed using diffusion-weighted imaging, T2WI, FLAIR imaging, and T2*WI sequences (details on MRI sequence parameters are included in the Supplemental material). The time (h) between stroke onset and CT and MRI scans on admission were recorded for each patient. The imaging findings of all patients were reviewed by two neurologists who were blinded to the condition of the participants. Hematomas were classified according to their location in the putamen, thalamus, lobe, other regions (such as the caudate nucleus) and infratentorial regions (brain stem and cerebellum). As a characteristic form of hematoma, we assessed the presence or absence of a niveau formation on CT (Fig. 1A). As a perihematomal finding, we measured and recorded the maximum diameter (mm) of the perihematomal LDA using

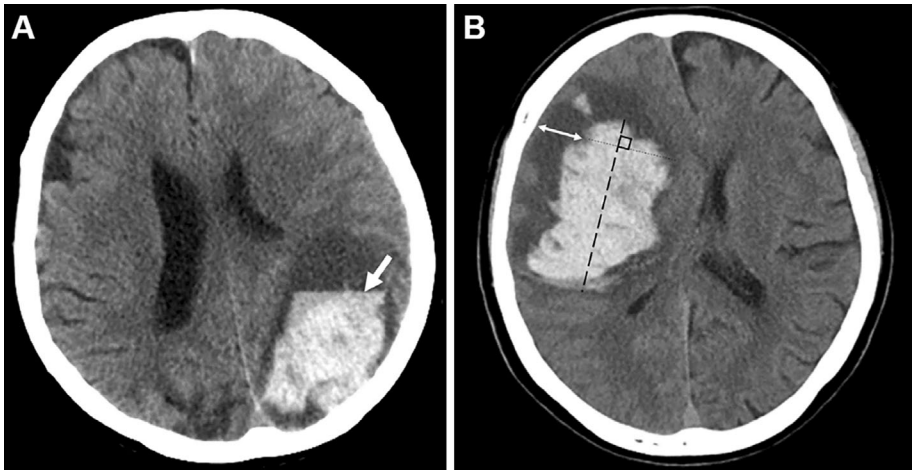

Figure 1. Hematoma visualization on CT. A: Niveau formation in the hematoma corresponding to the horizontal edge of a high-density area of the hematoma on CT (white arrow). B: The maximum diameter of the perihematomal LDA was measured perpendicularly to the maximum meridian of the hematoma on the slice image with the largest perihematomal LDA (maximum diameter: white double-headed arrow, maximum meridian of the hematoma: black dotted line). CT: computed tomography, LDA: low-density area

the centimeter scale on the CT scans. This was measured perpendicularly to the maximum meridian of the hematoma on the slice image containing the largest perihematomal LDA (Fig. 1B).

Measurement of ICH and edema volumes

We directly measured the ICH and perihematomal edema (PHE) volumes on CT and MRI scans using version 4.80 of 3D-Slicer, which is a free, open-source software platform for visualization and medical image computing (https://www.slicer.org) (14). The ICH volume on CT images was measured by tracing the HDA of the hematoma using the level tracing segment editor tool. The hematoma was automatically identified in each slice, pixel by pixel, after setting the range between 40 and 100 Hounsfield units (HU) (14, 15). The ICH and PHE volumes on MRI scans were evaluated based on FLAIR images (16) and then were manually measured by tracing the edges of hematoma lesions and the perihematomal hyper-intensity areas using the free-hand drawing tool. We obtained a follow-up CT scan within 24 hours of the CT performed at the time of admission and evaluated the presence or absence of hematoma growth. Significant hematoma growth was classified and defined as an increase of >6 cm^3 or >12.5 cm^3 in size or >33% in ICH volume on the follow-up CT scan, based on past reports (17, 18).

CT perihematomal rim

The imaging characteristics of a CT perihematomal rim are shown in Fig. 2. The CT perihematomal rim showed a high-intensity signal that is similar to that of the cerebrospinal fluid (CSF) on T2WI and an iso-intensity signal that is similar to that of the cerebral parenchyma on FLAIR imaging. It was located inside the hypo-intense rim at the edge of the hematoma on T2*WI. CT perihematomal rims were often distributed above or to the sides of the hematomas, and hematoma growth was observed within the CT perihematomal rims in some cases (Supplementary material). We specifically defined a CT perihematomal rim as a perihematomal low-density lesion on CT corresponding to (a) a clear high-intensity signal on MRI T2WI, (b) an iso-intensity signal similar to cerebral parenchyma on FLAIR imaging, and (c) reflected as a hypo-intense rim surrounding the hematoma on T2*WI.

Statistical analysis

All statistical analyses were performed using a commercially available software package (IBM SPSS, version 25.0). We divided the participants according to the presence or absence of a CT perihematomal rim and compared imaging findings between the CT perihematomal rim-positive and -negative groups. Next, we determined the volumetric differences in ICH (cm^3) between the MRI and CT scans and assessed their relationship with the presence of CT perihematomal rims. At the same time, we performed univariate and multivariate logistic regression analyses to assess whether CT findings were able to predict the presence of a CT perihematomal rim. We used the chi-square test to compare the proportions of categorical variables (e.g., sex) and the Mann-Whitney *U* test to compare the means or medians of continuous variables (e.g., age). A p value <0.05 was considered to be statistically significant. A receiver operating characteristic (ROC) analysis was performed to assess the maximum diameter threshold of the perihematomal LDA on CT images, which could predict the presence of a CT perihematomal rim. The inter-observer reliability of imaging findings was determined by deriving the intraclass correlation coefficient (ICC) and Kappa ($\varkappa$) values (the classifica-

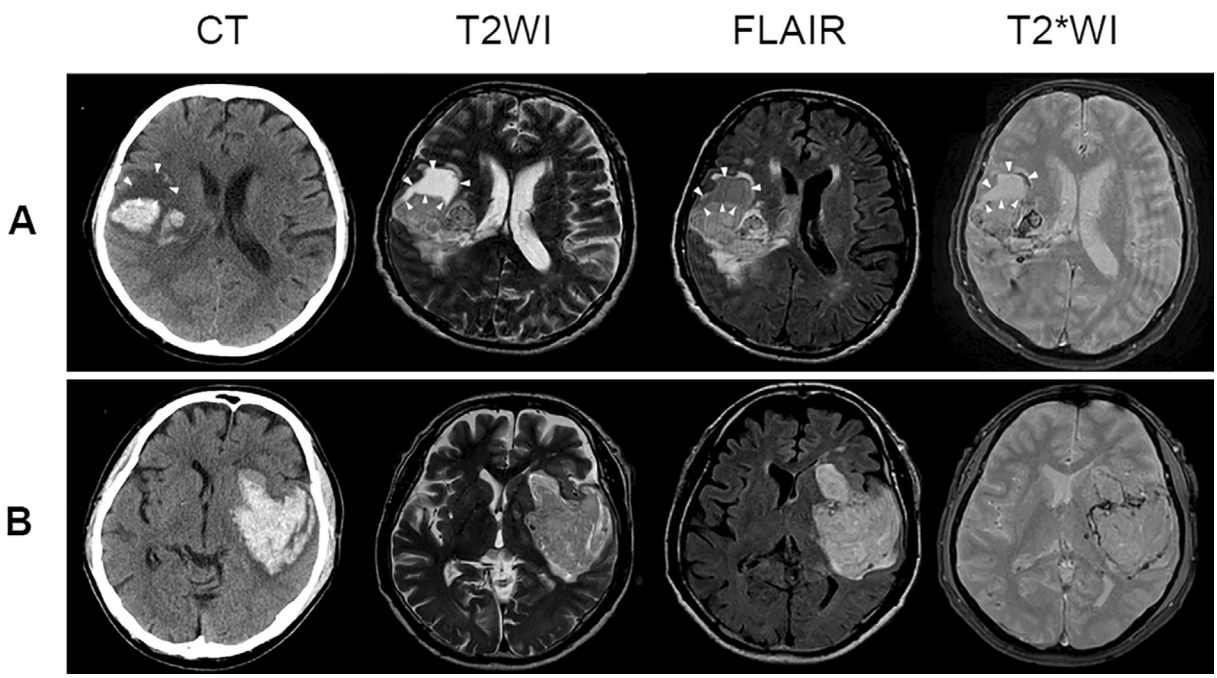

Figure 2. **Comparison of acute ICH lesion images with (A) and without (B) a CT perihematomal rim. A: The CT perihematomal rim is visualized as a perihematomal low density lesion on the CT image (furthest left, white arrowheads). This finding shows an intensity signal similar to that of cerebrospinal fluid in MRI T2-weighted images (second from left, white arrowheads) and an iso-intensity signal similar to that of cerebral parenchyma in FLAIR images (third from left, white arrowheads), and it is surrounded by a hypo-intense rim around the hematoma in GRE T2*-weighted images (furthest right, white arrowheads). B: Comparative images of an acute ICH lesion without a CT perihematomal rim. CT: computed tomography, FLAIR: fluid-attenuated inversion recovery, GRE: gradient recalled echo, ICH: intracerebral hemorrhage, MRI: magnetic resonance imaging**

tion of ICC and $\varkappa$ values are included in the Supplementary material).

Results

We included 139 patients (91 men, 48 women) with a mean ± standard deviation age of 66±13 years in the study. The median (interquartile range) ICH volumes on CT and MRI were 6.33 (3.32-16.88) cm^3 and 8.48 (3.91-21.95) cm^3, respectively. CT perihematomal rims were observed in 40 of the 139 patients (29%). The baseline characteristics of the patients in the CT perihematomal rim -positive (n=40) and -negative (n=99) groups are listed in Table 1. There were no significant differences in sex, age, life history, disease history, and drug history between the two groups. Serum CRP, plasma D-dimer, and plasma BNP levels were not significantly different between the two groups. NIHSS scores on admission and worst NIHSS scores during hospitalization were significantly higher in the CT perihematomal rim-positive group than in the CT perihematomal rim-negative group. Conversely, a poor functional outcome was not significantly different (positive vs. negative group: 50% vs. 41%, p=0.356). The baseline ICH volumes on CT and MRI scans were significantly larger in the CT perihematomal rim-positive group than in the CT perihematomal rim-negative group (CT: 19.31 cm^3 vs. 4.90 cm^3, p<0.001; MRI: 26.06 cm^3 vs. 5.37 cm^3, p<0.001). The proportion of patients with hematoma growth >6 cm^3 was significantly higher in the CT perihematomal rim-positive group than in the CT perihematomal rim-negative group (18% vs. 4%, p=0.006). On the other hand, there were no significant differences in the hematoma growth of >12.5 cm^3 or >33% between the groups. The maximum diameter of the perihematomal LDAs on CT and the PHE volume on MRI were significantly greater in the CT perihematomal rim-positive group than in the CT perihematomal rim-negative group (LDA: 12.12 mm vs. 5.64 mm, p<0.001; PHE: 17.59 cm^3 vs. 5.73 cm^3, p< 0.001). Furthermore, the CT perihematomal rim volume was significantly associated with the PHE volume on MRI (Pearson's correlation coefficient: 0.547, p<0.001) hemorrhages. Most patients in the CT perihematomal rim-positive group had a supratentorial hemorrhage, and the presence of a CT perihematomal rim was significantly associated with the putamen (positive vs. negative group: 63% vs. 35%, p=0.003) and lobar hematomas (positive vs. negative group: 35% vs. 13%, p=0.003). Moreover, a niveau formation in the hematoma was strongly associated with the presence of a CT perihematomal rim (positive vs. negative group: 58% vs. 2%, p<0.001). Finally, the median time from ICH onset to admission for CT and MRI scanning was significantly

Table 1. Comparison of the Baseline Characteristics Included in the Univariate Analysis between the CT Perihematomal Rim-positive and -negative Groups.

Variable	Total (n=139)	CT perihematomal rim-positive group (n=40)	CT perihematomal rim-negative group (n=99)	p value
Age in years, mean±SD	66±13	65±13	67±13	0.533
Male, n (%)	91 (65%)	28 (70%)	63 (63%)	0.475
Smoking, n (%)	66 (47%)	16 (40%)	50 (50%)	0.353
Alcohol use, n (%)	92 (66%)	28 (70%)	65 (66%)	0.749
Hypertension, n (%)	82 (59%)	26 (65%)	56 (57%)	0.360
Diabetes, n (%)	27 (19%)	8 (20%)	19 (19%)	0.913
Dyslipidemia, n (%)	64 (46%)	14 (35%)	50 (51%)	0.097
Atrial fibrillation, n (%)	14 (10%)	4 (10%)	10 (10%)	0.986
Antiplatelet use, n (%)	14 (10%)	6 (15%)	8 (8%)	0.208
Anticoagulant use, n (%)	16 (12%)	3 (8%)	13 (13%)	0.359
CRP in mg/dL, mean (SD)	0.08 (0.04-0.19)	0.09 (0.05-0.28)	0.08 (0.04-0.18)	0.412
D-dimer in μg/mL, mean (SD)	0.80 (0.60-1.10)	0.80 (0.60-1.58)	0.75 (0.60-1.00)	0.406
BNP in pg/mL, mean (SD)	38.8 (17.1-78.9)	45.0 (25.1-98.1)	35.3 (14.7-71.4)	0.188
Admission SBP in mmHg, mean±SD	179±29	179±25	179±31	0.976
Admission DBP in mmHg, mean±SD	99±19	95±16	101±20	0.137
NIHSS score on admission, median (IQR)	8 (4-15)	15 (6-18)	7 (4-13)	0.003
Worst NIHSS score, median (IQR)	10 (4-17)	16 (7-19)	8 (4-15)	0.003
Poor clinical outcome, n (%)	61 (44%)	20 (50%)	41 (41%)	0.356
Surgical hematoma removal, n (%)	11 (8%)	6 (15%)	5 (5%)	0.051
Hematoma location				
Putamen, n (%)	60 (43%)	25 (63%)	35 (35%)	0.003
Thalamus, n (%)	38 (27%)	0 (0%)	38 (38%)	<0.001
Lobar, n (%)	27 (19%)	14 (35%)	13 (13%)	0.003
Other, n (%)	2 (1%)	0 (0%)	2 (1%)	0.365
Infratentorial hemorrhage, n (%)	12 (9%)	1 (3%)	11 (11%)	0.102
Niveau formation in the hematoma, n (%)	25 (18%)	23 (58%)	2 (2%)	<0.001
Baseline ICH volume on CT in cm^3, median (IQR)	6.33 (3.32-16.88)	19.31 (12.19-53.91)	4.90 (2.38-8.48)	<0.001
Baseline ICH volume on MRI in cm^3, median (IQR)	8.48 (3.91-21.95)	26.06 (15.60-68.79)	5.37 (2.64-12.06)	<0.001
Hematoma growth>6 cm^3 in size, n (%)	11 (8%)	7 (18%)	4 (4%)	0.006
Hematoma growth>12.5 cm^3 in size, n (%)	4 (3%)	2 (5%)	2 (2%)	0.324
Hematoma growth>33% in ICH volume, n (%)	9 (6%)	2 (5%)	7 (7%)	0.682
Maximum perihematomal LDA diameter in mm, median (IQR)	6.45 (4.86-8.99)	12.12 (8.26-14.84)	5.64 (4.09-6.91)	<0.001
PHE volume on MRI, median (IQR)	7.01 (3.81-15.63)	17.59 (7.97-29.09)	5.73 (2.97-8.94)	<0.001
Cerebral microbleeds number, median (IQR)	2 (0-5)	2 (0-3)	3 (0-6)	0.063
Intraventricular hemorrhage, n (%)	41 (30%)	10 (25%)	31 (31%)	0.460
Time to admission CT in h, median (IQR)	2.6 (1.6-6.4)	3.0 (2.1-9.6)	2.2 (1.6-5.8)	0.027
Time to admission MRI in h, median (IQR)	2.5 (1.7-6.6)	3.3 (2.2-9.8)	2.3 (1.5-6.1)	0.019

BNP: brain natriuretic peptide, CRP: C-reactive protein, CT: computed tomography, DBP: diastolic blood pressure, ICH: intracerebral hemorrhage, IQR: inter quartile range, LDA: low-density area, MRI: magnetic resonance imaging, NIHSS: National Institutes of Health Stroke Scale, PHE: perihematomal edema, SBP: systolic blood pressure, SD: standard deviation

greater, by 3 hours or more, in the CT perihematomal rim-positive group than in the CT perihematomal rim-negative group (CT: 3.0 hours vs. 2.2 hours, p=0.027; MRI: 3.3 hours vs. 2.3 hours, p=0.019). The median time difference between MRI and CT was not significantly different between the two groups, while both were negative values (-0.15 hours vs. -0.20 hours, p=0.200).

Scatter plots showing the baseline ICH volume distributions in patients with and without CT perihematomal rim are presented in Fig. 3. The ICH volume on MRI was larger than that on a CT in most patients who had a CT perihematomal rim; the approximately straight line in Fig. 3 shows the shifted distribution from a 1:1 fitted line. The Mann-Whitney *U* test revealed that differences in ICH volumes between MRI and CT were significantly larger in patients who had a CT perihematomal rim than in those who did not (7.19 cm^3 vs. 1.03 cm^3, p<0.001). Furthermore, the differences in the ICH volumes between MRI and CT showed a strong positive correlation with the hematoma volumes on CT (Pearson's correlation coefficient: r=0.818, p<0.001). Furthermore, the median ratio of ICH volumes estimated by CT to that by MRI (CT/MRI) was significantly lower in patients who had a CT perihematomal rim than in those who did not [0.70 (0.61-0.80) vs. 0.80 (0.71-0.91), p<0.001], and

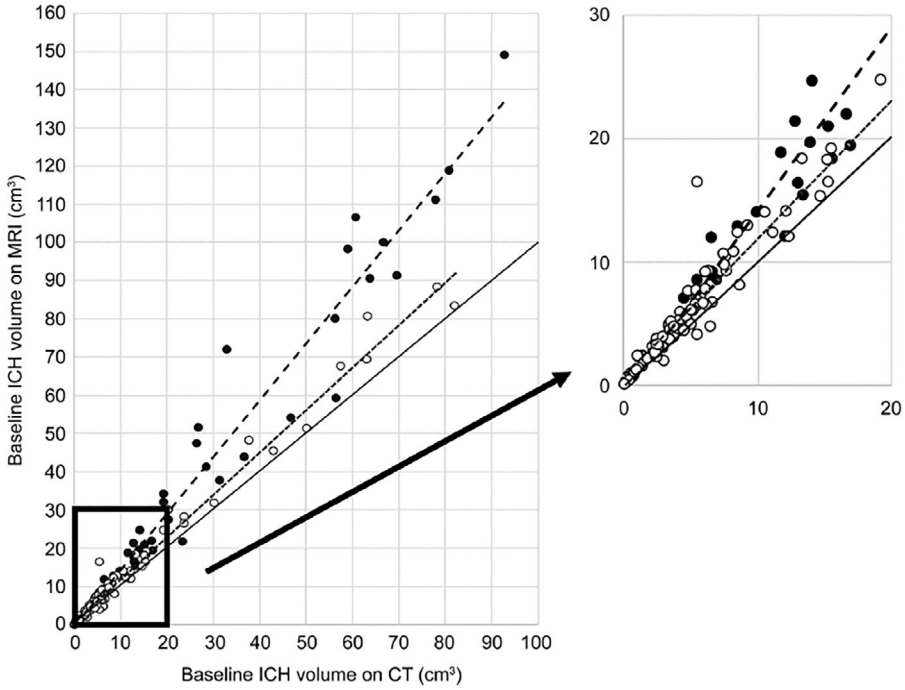

Figure 3. **Scatter plots showing the distribution of the baseline ICH volumes in patients with and without a CT perihematomal rim. Each coordinate represents an individual hematoma volume on CT and MRI. Black coordinates: baseline ICH volumes in patients with a CT perihematomal rim. White coordinates: baseline ICH volumes in patients without a CT perihematomal rim. Black solid line: 1: 1 fitted line indicating the baseline ICH volumes on CT and MRI. Black dotted line: approximate straight-line showing the coordinates of patients with a CT perihematomal rim. Gray dotted line: approximate straight line reflecting the coordinates of patients without a CT perihematomal rim. An approximate straight-line reflecting the coordinates of patients without a CT perihematomal rim was the best fit with a 1: 1 fitted line on linear regression analysis (R^2=0.991). CT: computed tomography, ICH: intracerebral hemorrhage, MRI: magnetic resonance imaging**

Table 2. **Multivariate Analysis of the Factors Related to CT Perihematomal Rims.**

Variable	Odds ratio	95% confidence interval	p value
NIHSS score on admission	1.032	0.932-1.143	0.539
Time to the admission CT scan	0.972	0.871-1.085	0.618
Putamen hemorrhage	9.172	1.847-45.531	0.007
Baseline hematoma volume on CT	1.000	0.967-1.035	0.982
Niveau formation in the hematoma	21.703	3.192-147.553	0.002
Maximum perihematomal LDA diameter	1.659	1.238-2.223	0.001

CT: computed tomography, LDA: low-density area, NIHSS: National Institutes of Health Stroke Scale

the ICH volumes on CT were 30% lower than those on MRI.

Several variables that were significant (p<0.05) in the univariate analysis (NIHSS score on admission, time to the admission CT scan, putamen hemorrhage, baseline hematoma volume on CT, niveau formation in the hematoma, and maximum perihematomal LDA diameter) were retained in the multivariate logistic model. In the multivariate logistic regression analysis, putamen hemorrhage (p=0.007), niveau formation in the hematoma (p=0.002), and maximum perihematomal LDA diameter (p=0.001) were independent factors related to CT perihematomal rims (Table 2). In the ROC analysis, the maximum diameter threshold of the perihematomal LDA for the presence of a CT perihematomal rim was 7.5 mm, and the sensitivity and specificity were 85% and 83%, respectively. The percentage of patients who had a CT perihematomal rim was significantly higher among those who had a large perihematomal LDA (>7.5 mm, n=50) than among those who had a small perihematomal LDA (≤7.5 mm, n=89; 66% vs. 8%, p<0.001; Fig. 4).

Furthermore, we classified the perihematomal regions according to four distinct areas (ventral, lateral cortical, lateral ventricular, and dorsal) and evaluated the distribution of patients across these areas according to CT perihematomal rim location (Supplementary material). This analysis revealed that CT perihematomal rims were distributed across all four

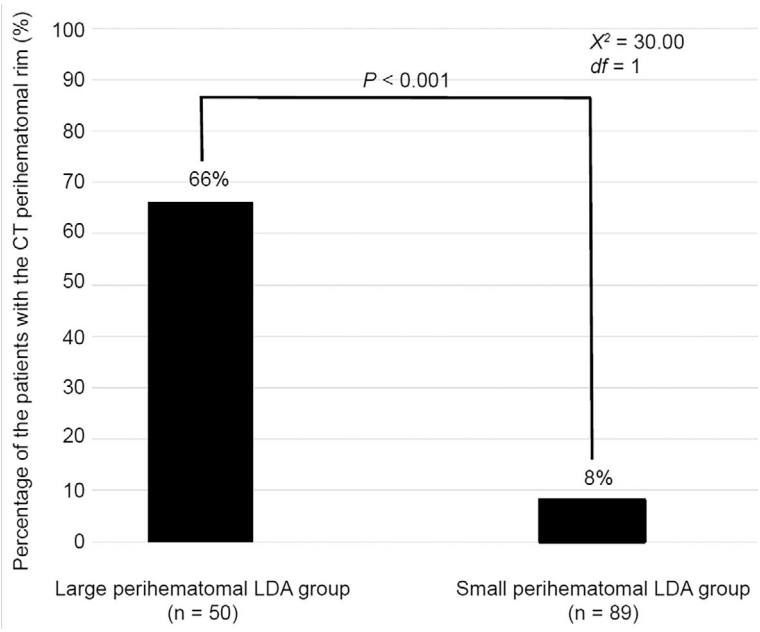

Figure 4. Percentage of patients with a CT perihematomal rim among those with large (>7.5 mm) and small (≤7.5 mm) perihematomal LDAs. CT: computed tomography, χ2: chi-square, df: degrees of freedom, LDA: low-density area

regions, with the greatest frequency observed in the ventral and lateral cortical aspects [n=32 (80%) and n=19 (48%), respectively], and the lowest frequency in the lateral ventricular and dorsal aspects [n=8 (20%) and n=7 (18%), respectively] (Supplementary material).

Discussion

We observed perihematomal low-density lesions by CT that appeared to be part of hemorrhagic regions on MRI in 29% of the patients with acute ICH and named them "CT perihematomal rim." The median ratio of the ICH volume (CT/MRI) was significantly lower in patients with a CT perihematomal rim than in those without, and the ICH volume on CT was 30% lower than that on MRI. According to multivariate logistic regression analyses, the presence of a CT perihematomal rim was independently associated with putamen hemorrhage, niveau formation in the hematoma, and maximum perihematomal LDA diameter.

The CT perihematomal rim shows the imaging characteristics of a liquid component (T2 high-intensity signal similar to CSF, niveau formation, etc.); however, it shows no loss of signal on FLAIR imaging. Moreover, the CT perihematomal rim was likely to be mainly found on the ventral aspect within a hematoma at 3 or more hours following ICH onset, with clot retraction being known as a change in hematoma components at about the same time (5, 12, 19-21). Several reports have noted a horizontal fluid-fluid level and linear gradient (low-density layering ventrally and high-density layering dorsally) within acute hematomas on CT (19, 20, 22). One of the factors that affect the visualization of blood components on CT is the hematocrit (Ht) value (23), and this phenomenon is considered to reflect the bilayer distribution of blood components according to their different Ht values after clot retraction (upper serum components with low Ht values and lower blood cell components with high Ht values) and this is called the "hematocrit effect" (22). Therefore, we suspected that a CT perihematomal rim reflects the separated serum components in an acute hematoma by clot retraction.

We also considered the relationship between the distribution of the CT perihematomal rim and the location of the ICH lesion. In our study, CT perihematomal rims were mostly observed ventrally and laterally to the hematoma, i.e., its cortical side, but less frequently medially or dorsally, i.e., at the ventricular side of a hematoma. Further, CT perihematomal rims were more commonly localized in the putamen and lobar hematomas but less commonly so in thalamic and infratentorial hematomas. The location of an ICH lesion is one of the major factors affecting hematoma formation (24-27); on the other hand, little is known about the relationship of an ICH lesion with the distribution of blood components within a hematoma. A possible explanation for our findings is that differences in mechanical properties of brain tissues due to varying nerve fiber densities influences the distribution of blood components within the hematoma. In the supratentorial regions, lobar hemorrhages form larger hematomas than do deeper hemorrhages owing to the low density of nerve fibers (28). Putamen hemorrhages form in the same brain regions relatively larger hematomas than do thalamic hemorrhages (29) owing to the influence of the relatively lower density of nerve fibers in the putamen (30, 31). Based on these histological characteristics, putamen and lobar hemorrhages might more easily form large hematomas with high serum content, and the separated serum components might be more likely recognized as a "CT

perihematomal rim" on the cortical side where hematomas are likely to spread due to the lower nerve fiber density.

In this study, we were able to clearly identify CT perihematomal rims and their imaging characteristics by combining CT and multisequence MRI, which is known to be useful for acute ICH diagnosis (8, 10, 32). Furthermore, using an imaging analysis software program (3D-Slicer) (14), we measured the ICH volume on CT and MRI scans, regardless of the specific characteristics (shape, etc.) of the hematoma. The presence of a CT perihematomal rim confirms that the actual acute intracerebral hemorrhagic volume is larger than the calculated hematoma volume based on the HDA on CT. We evaluated the maximum diameter of perihematomal LDA on CT as an index to judge the existence of a CT perihematomal rim that can be easily used in a clinical setting. Based on our results, a large perihematomal LDA (>7.5 mm) on CT in acute ICH cases should be considered a CT perihematomal rim. In this case, CT may have underestimated the ICH volume by 30%.

There are some limitations associated with our study. First, the number of participants was limited because we excluded several who were unable to undergo MRI scanning due to severe symptoms (such as vomiting, consciousness disturbance, etc.). As a result, various patients with severe bleedings were excluded, and the relationship between CT perihematomal rim and either hematoma expansion or a poor outcome may not have been accurately assessed. Second, we do not routinely use quantitative susceptibility mapping which is useful for the quantitative assessment of hematoma lesions (33); therefore, we did not have the most accurate hematoma volume assessment. Third, there were large variations in the elapsed time from ICH onset to the imaging examinations among patients; thus, we could not evaluate the imaging findings in a unified time window. Finally, our study only included patients from a single center; therefore, we could not verify the applicability of our findings to patients from other centers.

Conclusion

We observed perihematomal low-density lesions on CT that appeared to form part of hemorrhages on MRI in 29% of patients with acute ICH; we named these lesions "CT perihematomal rims." This finding may reflect the serum components separated by clot retraction in acute hematomas. The presence of a CT perihematomal rim suggests that the actual acute ICH volume is larger than it appears on CT; in this study, CT underestimated the ICH volume by approximately 30%. A large perihematomal LDA (>7.5 mm) on CT in acute ICH cases is therefore considered to be a CT perihematomal rim.

The authors state that they have no Conflict of Interest (COI).

Acknowledgement

We would like to thank the entire medical staff at the Departments of Neurology and Radiology and the Graduate School of Medicine of Nippon Medical School, Tokyo, Japan.

References

1. Adams Jr HP, Adams RJ, Brott T, et al. Guidelines for the early management of patients with ischemic stroke: a scientific statement from the Stroke Council of the American Stroke Association. Stroke **34**: 1056-1083, 2003.
2. Kothari RU, Brott T, Broderick JP, et al. The ABCs of measuring intracerebral hemorrhage volumes. Stroke **27**: 1304-1305, 1996.
3. Urday S, Beslow LA, Goldstein DW, et al. Measurement of perihematomal edema in intracerebral hemorrhage. Stroke **46**: 1116-1119, 2015.
4. Urday S, Beslow LA, Dai F, et al. Rate of perihematomal edema expansion predicts outcome after intracerebral hemorrhage. Crit Care Med **44**: 790-797, 2016.
5. Huisman TA. Intracranial hemorrhage: ultrasound, CT and MRI findings. Eur Radiol **15**: 434-440, 2005.
6. Zhu C, Jiang T. Multicontext fuzzy clustering for separation of brain tissues in magnetic resonance images. Neuroimage **18**: 685-696, 2003.
7. Patel MR, Edelman RR, Warach S. Detection of hyperacute primary intraparenchymal hemorrhage by magnetic resonance imaging. Stroke **27**: 2321-2324, 1996.
8. Schellinger PD, Jansen O, Fiebach JB, Hacke W, Sartor K. A standardized MRI stroke protocol: comparison with CT in hyperacute intracerebral hemorrhage. Stroke **30**: 765-768, 1999.
9. Kidwell CS, Chalela JA, Saver JL, et al. Comparison of MRI and CT for detection of acute intracerebral hemorrhage. JAMA **292**: 1823-1830, 2004.
10. Linfante I, Linas RH, Caplan LR, Warach S. MRI features of intracerebral hemorrhage within 2 hours from symptom onset. Stroke **30**: 2263-2267, 1999.
11. Noguchi K, Seto H, Kamisaki Y, Tomizawa G, Toyoshima S, Watanabe N. Comparison of fluid-attenuated inversion-recovery MR imaging with CT in a simulated model of acute subarachnoid hemorrhage. Am J Neuroradiol **21**: 923-927, 2000.
12. Cordonnier C, Demchuk A, Ziai W, Anderson CS. Intracerebral haemorrhage: current approaches to acute management. Lancet **392**: 1257-1268, 2018.
13. Cowie MR, Struthers AD, Wood DA, et al. Value of natriuretic peptides in assessment of patients with possible new heart failure in primary care. Lancet **350**: 1349-1353, 1997.
14. Xu X, Chen X, Zhang J, et al. Comparison of the Tada formula with software slicer: precise and low-cost method for volume assessment of intracerebral hematoma. Stroke **45**: 3433-3435, 2014.
15. Nowinski WL, Gomolka RS, Qian G, Gupta V, Ullman NL, Hanley DF. Characterization of intraventricular and intracerebral hematomas in non-contrast CT. Neuroradiol J **27**: 299-315, 2014.
16. Venkatasubramanian C, Mlynash M, Finley-Caulfield A, et al. Natural history of perihematomal edema after intracerebral hemorrhage measured by serial magnetic resonance imaging. Stroke **42**: 73-80, 2011.
17. Demchuk AM, Dowlatshahi D, Rodriguez-Luna D, et al. Prediction of hematoma growth and outcome in patients with intracerebral hemorrhage using the CT-angiography spot sign (PREDICT): a prospective observational study. Lancet Neurol **11**: 307-314, 2012.
18. Brouwers HB, Greenberg SM. Hematoma expansion following acute intracerebral hemorrhage. Cerebrovasc Dis **35**: 195-201, 2013.
19. Parizel P, Makkat S, Van Miert E, Goetherm JV, van den Hauwe L, De Schepper AM. Intracranial hemorrhage: principles of CT

and MRI interpretation. Eur Radiol **11**: 1770-1783, 2001.
20. Xi G, Keep RF, Hoff JT. Pathophysiology of brain edema formation. Neurosurg Clin N Am **13**: 371-383, 2002.
21. Klahr AC, Kate M, Kosior J, et al. Early hematoma retraction in intracerebral hemorrhage is uncommon and does not predict outcome. PLoS ONE **13**: e0205436, 2018.
22. Le TH, Gean AD. Imaging of head trauma. Semin Roentgenol **41**: 177-189, 2006.
23. Trans JT. Computed tomography of intracerebral hematoma. Clin Neurol Neurosurg **79**: 285-295, 1976.
24. Chen R, Wang X, Anderson CS, et al. Infratentorial intracerebral hemorrhage. Stroke **50**: 1257-1259, 2019.
25. Fewel ME, Thompson BG, Hoff JT. Spontaneous intracerebral hemorrhage: a review. Neurosurg Focus **15**: E1, 2003.
26. Falcone GJ, Biffi A, Brouwers HB, et al. Predictors of hematoma volume in deep and lobar supratentorial intracerebral hemorrhage. JAMA Neurol **70**: 988-994, 2013.
27. Roh D, Sun CH, Murthy S, et al. Hematoma expansion differences in lobar and deep primary intracerebral hemorrhage. Neurocrit Care **31**: 40-45, 2019.
28. Yogendrakumar V, Demchuk AM, Aviv RI, et al. Location of intracerebral haemorrhage predicts haematoma expansion. Eur Stroke J **2**: 257-263, 2017.
29. Hier DB, Babcock DJ, Foulkes MA, Mohr JP, Price TR, Wolf PA. Influence of site on course of intracerebral hemorrhage. J Stroke Cerebrovasc Dis **3**: 65-74, 1993.
30. Herrero MT, Barcia C, Navarro JM. Functional anatomy of thalamus and basal ganglia. Childs Nerv Syst **18**: 386-404, 2002.
31. Nakagawa K, King SL, Seto TB. Optimal hematoma volume cut points to predict functional outcome after basal ganglia and thalamic hemorrhage. Front Neurol **9**: 291, 2018.
32. Fiebach JB, Schellinger PD, Gass A, et al. Stroke magnetic resonance imaging is accurate in hyperacute intracerebral hemorrhage: a multicenter study on the validity of stroke imaging. Stroke **35**: 502-506, 2004.
33. Wang S, Lou M, Liu T, Cui D, Chen X, Wang Y. Hematoma volume measurement in gradient echo MRI using quantitative susceptibility mapping. Stroke **44**: 2315-2317, 2013.